Molecular Catalysis 449 (2018) 49–61

Contents lists available at ScienceDirect

Molecular Catalysis

journal homepage: www.elsevier.com/locate/mcat

Influence of anions and solvents on distinct coordination chemistry of cobalt and effect of coordination spheres on the biomimetic oxidation of *o*-aminophenols

Anangamohan Panja[a,*], Narayan Ch. Jana[a], Paula Brandão[b]

[a] Postgraduate Department of Chemistry, Panskura Banamali College, Panskura RS, WB 721152, India
[b] Department of Chemistry, CICECO-Aveiro Institute of Materials, University of Aveiro, 3810-193 Aveiro, Portugal

ARTICLE INFO

Keywords:
Cobalt complexes
Structural diversity
Biomimetic catalytic study
Influence of coordination sphere on catalytic activity
Mass spectrometry and plausible mechanism

ABSTRACT

The present work reports the synthesis and structural characterizations of five new cobalt complexes (**1–5**) resulting from a N_3O donor ligand, a Schiff base condensation product of *N,N*-dimethyldipropylenetriamine and 3-ethoxysalicylaldehyde, and their catalytic activity for the aerobic oxidation of various substrates, namely *o*-aminophenols and catechol. X-ray structural studies reveal that the Schiff base ligand can bind the metal centre either in the tetradentate fashion using all the available donor sites of the monoanionic deprotonated form (in **2** and **3**) or in the tridentate fashion using the zwitterionic form of the Schiff base ligand with pendent quaternary amine nitrogen (in **1** and **4**). Additionally, the monoanionic deprotonated ligand can bind the metal centre in the tridentate fashion (in **4** and **5)** where the pendent tertiary amine nitrogen is involved in the intramolecular hydrogen bonding. All these adaptabilities associated with this triamine make it appealing candidate for exploration of the coordination chemistry with diverse structures. All complexes except compound **1** are efficient functional models for phenoxazinone synthase, and as expected the availability of labile sites at the first coordination sphere for the substrate, *o*-aminophenol, binding is the governing factor for higher catalytic activity in **2** and **3**. Requisite of the hydrogen bond acceptor centre as well as proton abstraction centre at the second coordination sphere behind the facile oxidation of the substrate were also explored (reactivity of **1** *versus* **4** and **5**). Moreover, the broader catalytic ability of these complexes was examined with substituted aminophenol and catechol as substrates, and the results were assembled and analysed. Furthermore, emphasis was given to get insight into the mechanistic pathway of functioning phenoxazinone synthase activity, well supported by the mass spectral study.

1. Introduction

Oxidation reaction plays a vital role in organic chemistry for the synthesis of fine organic chemicals as well as in manufacture of large-scale petrochemical compounds [1,2]. The majority of these industrial processes involve the stoichiometric oxidation with traditional oxidants, such as permanganate, dichromate and heavy metal oxides, thereby producing vast wastes which are causing environmental pollution. Pressure from society has placed restrictions on such industrial oxidation methods, with emphasis on the need for sustainable and environmentally friendly processes. As a result, a greater attention has been given on the development of novel and efficient catalytic processes with use of molecular oxygen as a sole oxidant, which is environmentally benign and show a high efficiency per weight of oxidant. However, the direct oxidation of organic substrates by molecular oxygen is a challenging tusk because of its kinetic restriction that is associated with conversion of triplet ground state to singlet state of oxygen, and most of the time selectivity does not reach to the desired level [3–6]. Nature has developed several metallo-oxidases to make controlled aerobic oxidations under highly mild conditions in which metalloenzymes activate molecular oxygen for the synthesis of numerous biochemically important compounds with great regio- and stereo-selectivity [7–9]. Bioinorganic chemists have paid a lot attention in unravelling the catalytic mechanism of these enzymes by means of a synthetic analogue approach [10–12]. This approach helps to get insight into the structures of the active sites and reactive intermediates and the mechanistic details of dioxygen activation and oxidation reactions occurring at the active sites [13–19]. Mechanistic studies are clearly a means of developing better synthetic methods, which in turn help in searching efficient catalysts as alternatives of traditional toxic

* Corresponding author.
E-mail address: ampanja@yahoo.co.in (A. Panja).

https://doi.org/10.1016/j.mcat.2018.02.013
Received 2 August 2017; Received in revised form 12 February 2018; Accepted 14 February 2018

industrial catalysts. Therefore, the application of various oxidative transformations involving metal catalysis to specific transformations of different organic substrates, such as aromatic hydrocarbons, alkanes, and oxygen-containing compounds, by molecular dioxygen and their mechanistic exploration is the subject of growing interest [20].

We are now involved in developing biomimetic catalysts for the oxidation of 3,5-di-*tert*-butylcatechol and *o*-aminophenol by molecular dioxygen, modelling the structures and functions of catechol oxidase [21,22] and phenoxazinone synthase [23,24]. The latter is a multi-copper metalloenzyme that catalyses the oxidative coupling of a wide variety of substituted *o*-aminophenols to phenoxazinone chromophore in the final step for the biosynthesis of actinomycin D in aerobic condition [25]. This potent antineoplastic agent actinomycin D is well known for its wide clinical application for the treatment of many tumours, including Wilm's tumour, where the phenoxazinone chromophore intercalates with DNA base-pairs, thereby abnormal functioning can be stopped by preventing the DNA dependent RNA synthesis [26,27]. The active site structures of several oxidase enzymes and the structures of their efficient synthetic analogues with transition metals [21–25,28–36] clearly suggest that the functional models must have labile or vacant coordination sites available for substrate binding as a primary requirement for the efficient *in vitro* catalysis. Therefore, the ligands with fewer donor centres could be the buffeting choice for the development of synthetic analogues. Transition metal complexes with Schiff base ligands have been provided a large number of enzymatic models mainly because of their synthetic simplicity, and thereby fine tuning of the catalytic activity may be achieved by modification of the coordination environment at the metal centre by judicious choice of amine and carbonyl parts of the Schiff bases. It is also well known that the extraordinary catalytic activity of metalloenzymes is mainly regulated by the participation of protein chain through the substrate recognition and stabilisation of the intermediates exploiting various noncovalent forces [37–39]. Therefore, the design and synthesis of coordination compounds beyond the first coordination sphere could be the right way of developing efficient biomimetic catalysts.

We have now started developing coordination chemistry with the Schiff base ligands derived from the triamine *N,N*-dimethyldipropylenetriamine as the coordination chemistry with this amine was almost unexplored [40]. Moreover, this amine may readily produce N_3O donor Schiff base ligands when reacts with salicylaldehyde or its derivative. Such ligands by the reaction with transition metal ions could produce synthetic analogues having either vacant or labile position(s) available for substrate binding. Furthermore, the presence of different kind of functionality in the Schiff base ligands derived from this amine, namely imine, amines (both secondary and tertiary), and phenol (from salicylaldehyde part), may allow fine tuning of the ligand field around the metal centre, leading to significant modification of the catalytic efficiency. In continuation to our long standing interest in searching better biomimetic catalysts [21–24], in this present work, Schiff base HL (Scheme 1) derived from *N,N*-dimethyldipropylenetriamine and 3-ethoxysalicylaldehyde was allowed to react with cobalt(II) salts in the presence of different counter ions, and finally we ended up with the isolation of five new cobalt complexes, $[Co(HL)_2](ClO_4)_3{\cdot}2H_2O$ (**1**), $[Co(L)(N_3)_2]$ (**2**), $[Co(L)(NCS)_2]$ (**3**), $[Co(HL)(L)][Co(NCS)_4]{\cdot}0{\cdot}5CH_3OH$ (**4**) and $[Co(L)_2]_2[Co(NCO)_4]$ (**5**). Their structural diversities and biomimetic catalytic activities with various substrates such as *o*-aminophenol, 2-amino-5-methylphenol and 3,5-di-*tert*-butylcatechol in aerobic condition have been critically analysed. Remarkably, the influence of solvents and counter ions on the diverse coordination chemistry of cobalt was observed. Moreover, the flexible donor property associated with *N,N*-dimethyldipropylenetriamine part of the Schiff base was also explored. Further emphasis was also given to get insight into the structure-property correlation to justify the reactivity trend of the complexes.

2. Experimental section

2.1. Materials and physical measurements

Reagent or analytical grade chemicals such as cobalt(II) nitrate hexahydrate, cobalt(II) perchlorate hexahydrate, *o*-aminophenol (OAPH), 2-amino-5-methylphenol, 3-ethoxysalicylaldehyde, and *N,N*-dimethyldipropylenetriamine were purchased from commercial sources and used as received. Solvents were also reagent grade and used without further purification.

Caution! Azide and perchlorate salts of metal complexes especially with organic ligands are potentially explosive. Only a small quantity of material should be prepared at a time and it should be handled with great care.

Elemental analyses for carbon, hydrogen and nitrogen were performed using a Perkin-Elmer 240C elemental analyser. IR spectra were recorded on a PerkinElmer Spectrum Two FTIR spectrophotometer in the range 400–4000 cm^{-1} with the samples prepared as KBr pellets. UV–vis spectrophotometric studies were carried out in an Agilent Carry-60 diode array UV–vis spectrophotometer at room temperature. Cyclic voltammetric studies were performed at room temperature in methanol with tetrabutylammonium perchlorate as a supporting electrolyte on a CH Instrument electrochemical workstation model CHI630E with three-electrodes assembly comprising of a platinum working electrode, a platinum wire auxiliary electrode and a Ag/AgCl reference electrode. Electrospray ionization mass spectra (ESI–MS positive) were recorded in a Micromass Q-tof-Micro Quadruple mass spectrophotometer.

2.2. Synthesis of the Schiff-base ligand (HL)

Tetradentate N_3O donor Schiff base ligand (HL) was synthesized by the condensation reaction of 1.0 mmol of *N,N*-Dimethyldipropylenetriamine (159 mg) and 1.0 mmol of 3-ethoxysalicylaldehyde (166 mg) in 20 ml of methanol (or acetonitrile). Mixture of these reactants in methanol was allowed to reflux for *ca.* 1 h, and then cooled. The *in situ* prepared Schiff base ligand was used directly for the synthesis of the subsequent metal complexes as described below.

2.3. Synthesis of $[Co(HL)_2](ClO_4)_3{\cdot}2H_2O$ (1)

Addition of $Co(ClO_4)_2{\cdot}6H_2O$ (0.730 g, 2.0 mmol) dissolved in 20 ml of methanol to the Schiff base ligand HL (2.0 mmol) solution at room temperature instantly produced a dark-brown solution. The mixture was stirred in air for 30 min during which time light brown powders separated out from the solution. It was collected by filtration and washed with mother liquor followed by methanol/ether and finally air dried. Yield: 0.867 g (85%). Dark-brown crystals suitable for X-ray analysis were obtained from slow evaporation of acetonitrile-methanol mixture of the complex at ambient temperature within few days. Anal. Calcd. for $C_{70}H_{128}Co_2N_{12}O_{35}Cl_6$: C 41.45%, H 6.36%, N 8.29%. Found: C 41.28%, H 6.42%, N 8.35%. FTIR (KBr, cm^{-1}): $\nu(N_3)$ 2050 *vs*; $\nu(C{=}N)$ 1632 s; $\nu(ClO_4)$ 624 s, 1104 *vs*.

2.4. Synthesis of $[Co(L)(N_3)_2]$ (2)

$Co(NO_3)_2{\cdot}6H_2O$ (291 mg, 1.0 mmol) and Schiff base ligand HL (1.0 mmol) were mixed together in 40 ml acetonitrile, and to the mixture 2 ml aqueous solution of sodium azide (130 mg, 2.0 mmol) was added with stirring. The resulting solution was then heated to reflux for about 30 min during which time colour of the solution changed to dark brown. The reaction mixture was then filtered and kept at ambient temperature for slow evaporation. Analytically pure dark-brown crystals suitable for X-ray diffraction study were separated out from the solution after few days, which was collected by filtration and washed with methanol/ether and air dried. Yield: 392 mg (86%). Anal. Calcd.

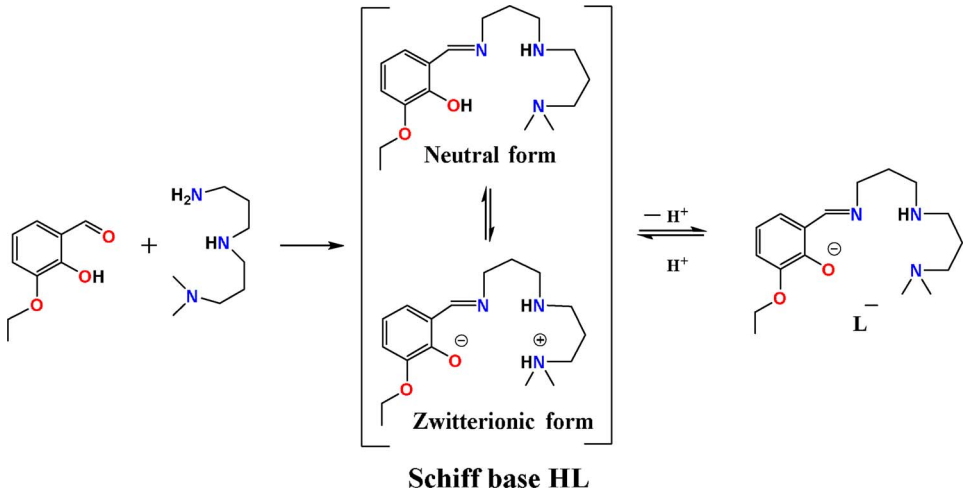

Scheme 1. Schiff base HL.

for $C_{17}H_{28}CoN_9O_2$: C 45.43%, H 6.28%, N 28.05%. Found: C 45.28%, H 6.25%, N 27.90%. FTIR (KBr, cm^{-1}): $\nu(N_3)$ 2050 *vs*; ν(C═N) 1632 s.

2.5. Synthesis of complex $[Co(L)(NCS)_2]$ (3)

Complex **3** was synthesized from an acetonitrile/water (20:1; v/v) mixture following a very similar procedure as described for **2,** except that NaSCN was used instead of NaN_3. Colour: Dark brown, Yield: 395 mg (83%). Anal. Calcd. for $C_{19}H_{28}CoN_5O_2S_2$: C 47.39%, H 5.86%, N 14.54%. Found: C 47.48%, H 5.80%, N 14.43%. FTIR (cm^{-1}, KBr): ν(NCS) 2107 s, ν(C═N) 1625 s.

2.6. Synthesis of complex $[Co(HL)(L)][Co(NCS)_4]\cdot 0{\cdot}5CH_3OH$ (4)

Complex **4** was synthesized from a methanol/water (20:1; v/v) mixture following the same methodology that applied for the synthesis of **2**, but NaSCN was used in place of NaN_3. Colour: Dark brown, Yield: 358 mg (72%). Anal. Calcd. for $C_{77}H_{118}Co_4N_{20}O_9S_4$: C 50.49%, H 6.49%, N 15.29%. Found: C 50.34%, H 6.50%, N 15.20%. FTIR (cm^{-1}, KBr): ν(NCS) 2064 s, ν(C═N) 1618 s.

2.7. Synthesis of complex $[Co(L)_2]_2[Co(NCO)_4]$ (5)

Complex **5** was synthesized from an acetonitrile/water (20:1; v/v) mixture adopting the identical procedure as described for **2,** except that NaNCO was used instead of NaN_3. Colour: Dark brown, Yield: 295 mg (78%). Anal. Calcd. for $C_{72}H_{112}Co_3N_{16}O_{12}$: C 55.06%, H 7.19%, N 14.27%. Found: C 55.19%, H 6.98%, N 14.28%. FTIR (cm^{-1}, KBr): ν(NCO) 2201 *vs*, ν(C═N) 1629 s.

2.8. X-ray crystallography

X-ray diffraction data for **1–5** were collected using monochromated Mo-Kα radiation (λ = 0.71073 Å) on a Bruker Smart Apex-II diffractometer, equipped with a CCD area detector. Multiple scans in φ and ω directions were made to increase the number of redundant reflections and were averaged during the refinement cycles. The images obtained during the data collection for all complexes were processed using the software SAINT-plus, and the multi-scan absorption correction method was then applied to minimize the absorption effects using SADABS program [41]. The structures were solved by the direct method and refined by the successive full-matrix least-squares cycles on F^2 using SHELXL-v.2013 or SHELXL-v.2014 [42]. All the non-hydrogen atoms were refined with anisotropic thermal parameters. Hydrogen atoms connected to carbon atoms were placed in geometrically idealized positions with fixed thermal parameters related to those they are attached (1.5 times for methyl hydrogens and 1.2 times for others). While hydrogen atoms connected to nitrogen atoms were located on the difference Fourier map and isotropically treated with given thermal parameters equivalent to 1.2 times of the parent atoms. Molecular graphics of **1–5** were generated with the programs like MERCURY-3.9. Detailed information related to crystallographic data collection and structure refinements are available in Table 1.

2.9. Catalytic oxidation of o-aminophenols/catechol

The catalytic oxidation of various substrates was carried out by the reaction of 1×10^{-4} M or 5×10^{-5} M of the complexes with 1.0×10^{-2} M substrates in air saturated methanol at room temperature. Kinetics of the aerobic oxidation of *o*-aminophenols catalysed by **1–5** were investigated monitoring increase of the absorbance as a function of time at their respective absorption maxima [43]. In order to determine dependence of the rate on the substrate concentration and to evaluate various kinetic parameters, 1×10^{-5} M solution of the complexes were subjected to react with at least 10 equivalents of the substrate maintaining the pseudo-first-order condition. All the kinetic measurements were carried out for the period of 10 min and the initial rate of the reaction was determined by the linear regression from slope of the absorbance verses time plots.

3. Results and discussion

3.1. Syntheses and general characterizations

Schiff base ligand HL was synthesized by the reaction of 3-ethoxysalicylaldehyde and *N,N*-dimethyldipropylenetriamine in a 1: 1 molar ratio in methanol (Scheme 1). This Schiff base ligand by the reaction with cobalt(II) perchlorate hexahydrate in a 2:1 molar ratio produced $[Co(HL)_2](ClO_4)_3\cdot 2H_2O$ (**1**) in high yield. Again treatment of this *in situ* generated Schiff base with cobalt(II) nitrate hexahydrate in the presence of pseudohalides (N_3^- for **2**, NCS^- for **3** and **4**, and NCO^- for **5**) in a 1:1:2 molar ratio produced $[Co(L)(N_3)_2]$ (**2**), $[Co(L)(NCS)_2]\cdot$ (**3**), $[Co(HL)(L)][Co(NCS)_4\cdot 0{\cdot}5CH_3OH$ (**4**) and $[Co(L)_2][Co(NCO)_4]$ (**5**), in high yield. Although the formation of these complexes was not dependent on the stoichiometric ratio of the reactants, the influence of solvents for the synthesis of distinct thiocyanate complexes (**3** *versus* **4**) was observed. Whereas the reaction of cobalt nitrate hexahydrate, Schiff base ligand, and sodium thiocyanate in acetonitrile/water mixture resulted only isolable product **3**; the same reaction from methanol/water mixture afforded only compound **4** in high yield. Starting with same reactants isolation of both **3** and **4** suggests that formation of the complexes is highly dependent on the solvents used for the synthesis,

Table 1
Crystal data and structure refinement parameters of complexes **1** to **5.**

	1	2	3	4	5
Empirical formula	$C_{35.5}H_{64}CoN_6O_{17.5}Cl_3$	$C_{17}H_{28}CoN_9O_2$	$C_{19}H_{28}CoN_5O_2S_2$	$C_{38.5}H_{59}Co_2N_{10}O_{4.5}S_4$	$C_{72}H_{112}Co_3N_{16}O_{12}$
Formula weight (g mol^{-1})	1014.21	449.41	481.51	980.05	1570.56
Temperature (K)	302(2)	150(2)	150(2)	150(2)	298(2)
Crystal system	Monoclinic	Monoclinic	Orthorhombic	Monoclinic	Tetragonal
Space group	$P2_1/n$	$P2_1/n$	$Pca2_1$	$P2_1/n$	$P4_2/n$
a (Å)	14.624(6)	14.919(2)	25.8819(5)	11.944(5)	17.2441(11)
b (Å)	13.434(5)	7.8906(11)	8.7010(4)	16.115(6)	17.2441(11)
c (Å)	24.005(7)	17.811(3)	9.7736(11)	24.762(10)	12.8049(8)
α (°)	90	90	90	90	90
b (°)	100.29(3)	96.642(5)	90	98.66(2)	90
γ (°)	90	90	90	90	90
volume (Å^3)	4640(3)	2082.6(5)	2201.0(3)	4712(3)	3807.7(5)
Z	4	4	4	4	2
D_{calc} (mg m^{-3})	1.437	1.430	1.453	1.382	1.370
μ (mm^{-1})	0.618	0.857	0.995	0.931	0.716
F(000)	2104	940	1008	2056	1666
θ Range (°)	2.147–28.346	1.687–25.851	2.341–27.162	1.513–25.543	2.848–26.394
Reflections collected	109337	15172	14693	42476	51321
Independent reflections (R_{int})	11555(0.0346)	3946(0.0456)	4784(0.0559)	8687(0.0750)	3893(0.0710)
Observed reflections [I > 2σ(I)]	7208	2978	3721	5370	3241
Restraints/parameters	0/591	0/269	1/268	1/564	0/271
Goodness-of-fit on F^2	1.052	1.061	1.010	1.066	1.183
Final *R* indices [I > 2σ(I)]	R_1 = 0.0809	R_1 = 0.0483	R_1 = 0.0410	R_1 = 0.0923	R_1 = 0.0850
	wR_2 = 0.2109	wR_2 = 0.1094	wR_2 = 0.0762	wR_2 = 0.2004	wR_2 = 0.1725
R indices (all data)	R_1 = 0.1274	R_1 = 0.0708	R_1 = 0.0645	R_1 = 0.1496	R_1 = 0.1029
	wR_2 = 0.2502	wR_2 = 0.1179	wR_2 = 0.0823	wR_2 = 0.2273	wR_2 = 0.1828
Largest diff. peak/hole (e Å^{-3})	0.599/–0.964	0.532/–0.416	0.370/–0.438	1.294/–0.866	0.693/–1.298

where the relative stabilities in a particular solvent system governs the identity of the species that crystallizes from that solvent. These observations establish that both of them are thermodynamic products and formation of them is controlled by the solvents used for their synthesis. As usual the metal centre connected to the Schiff base ligand was air-oxidized to cobalt(III) as found in the related complexes with similar ligand systems. All these complexes are sufficiently soluble in solvents like methanol, acetonitrile and DMF. The elemental analyses ensure the purity of the bulk samples, which are well matched with the X-ray crystallographic results.

In the IR spectra of all complexes, a sharp band is observed in the range 1615–1626 cm^{-1}, which are characteristic stretching vibrations of azomethine bond of the Schiff base. IR spectrum of **1** additionally shows board absorption bands at around 1080 and 624 cm^{-1}, which are assigned to the stretching and bending vibrations of perchlorate counter anion, respectively [44]. The broadening of ν(Cl—O) band is presumably due to the involvement of ClO_4^- ions in hydrogen bonding in the solid-state. IR spectrum of complex **2** displays a strong absorption band at 2033 cm^{-1}, which can be assigned to the stretching band of azide ion [45]. Complexes **3** and **4** show two stretching bands for thiocyanate ions at 2108 and 2067 cm^{-1}, respectively [46,47]. Lower stretching frequency of the thiocyanate ion in **4** is consistent with the greater π acceptor ability of thiocyanate from Co(II) centre compared to its π acceptor ability from Co(III) centre in **3**. Presence of cyanate ion in **5** was also confirmed by the observed stretching band at 2217 cm^{-1} [45].

3.2. Structural descriptions

Crystal structures of all complexes were determined by the single-crystal X-ray diffraction studies. Crystal structure of **1** along with selected atom numbering scheme is depicted in Fig. 1, the structures of **2** and **3** are shown in Fig. 2, while Figs. 3 and 4 represent the molecular structures of **4** and **5**, respectively. Structural parameters related to important bond distances around the metal coordination sphere for all structures are given in Table 2. Complex **1** crystallizes in the monoclinic $P2_1/c$ space group where the asymmetric unit consists of two

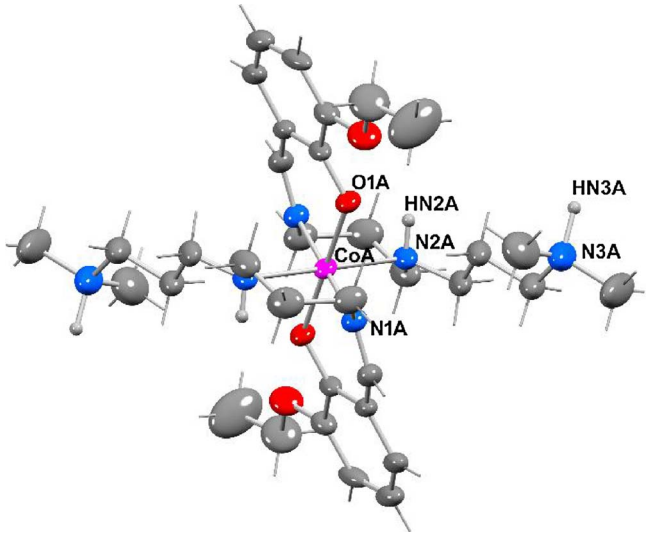

Fig. 1. Crystal structure of one of the crystallographically independent complex cations of **1** with selected atom numbering scheme. Thermal ellipsoids are drawn at 30% probability, and solvents are omitted for clarity.

crystallographically independent complex cations of formula $[Co(HL)_2]^{3+}$ on inversion centres, and two lattice water molecules and three perchlorate counter anions on general positions. Protonation of the tertiary amine nitrogen atom of the Schiff base is required to balance the charge of the system, and thus the zwitterionic form of the ligand is connected to the metal centre in **1**. The structure of both the crystallographically independent complex cations are eventually identical in that both the metal centres are hexacoordinated with distorted octahedral geometry. The coordination environments of the metal centres are fulfilled by one phenolate-O atom and both imine and secondary amine nitrogen atoms from each zwitterionic Schiff base ligand. The average Co—O and Co—N bond lengths are 1.895(3) and 1.982(4) Å which are typical for the low spin octahedral Co(III) complexes. The solid state structure of the complex is stabilised by strong hydrogen

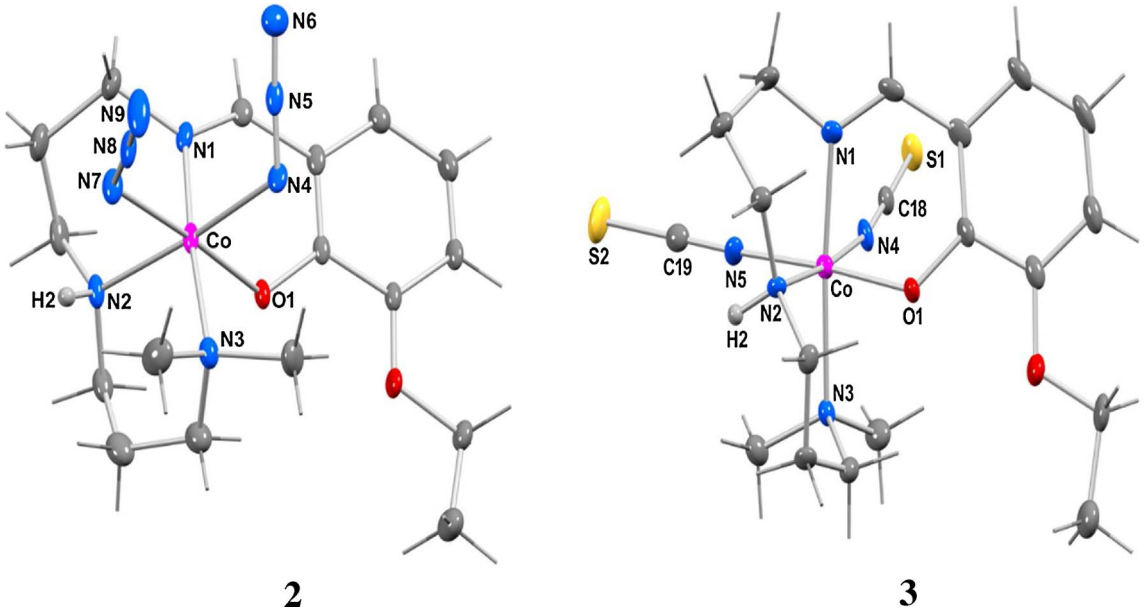

Fig. 2. Crystal structures of **2** and **3** showing selected atom numbering schemes. Thermal ellipsoids are drawn at 30% probability.

bonds involving the secondary and quaternary amines and lattice water molecules and perchlorate counter anions (Fig. S1).

Both **2** and **3** are neutral complexes and sit on general positions, but crystallize in the monoclinic $P2_1/n$ and orthorhombic $Pca2_1$ space groups, respectively. Both structures are eventually similar in which the central metal ions are hexacoordinated with slightly distorted octahedral geometry as suggested by the deviation of *cisoid* (84.07(11)–94.35(13)°) and *transoid* (173.66(11)–175.37(13)°) angles from the ideal values. The monoanionic Schiff base ligand (L) binds the metal centre through phenolate-O and three nitrogen atoms (one each of imine, secondary amine and tertiary amine nitrogen atoms) and two remaining coordination positions of the metal centre are connected with two nitrogen atoms of the terminal azides (in **2**) and thiocyanates (in **3**). In both cases, one meridional position is occupied by three nitrogen atoms from the triamine part of the Schiff base, while other one is occupied by two nitrogen atoms of pseudohalides and the phenolate-O atom of the Schiff base. The Co–N distances of pseudohalides and the Co–O distances of phenolate group of the tetradentate L ligand in **2** and **3** are found in the range 1.844(3)–1.895(2) and 1.912(5)–1.964(3) Å,

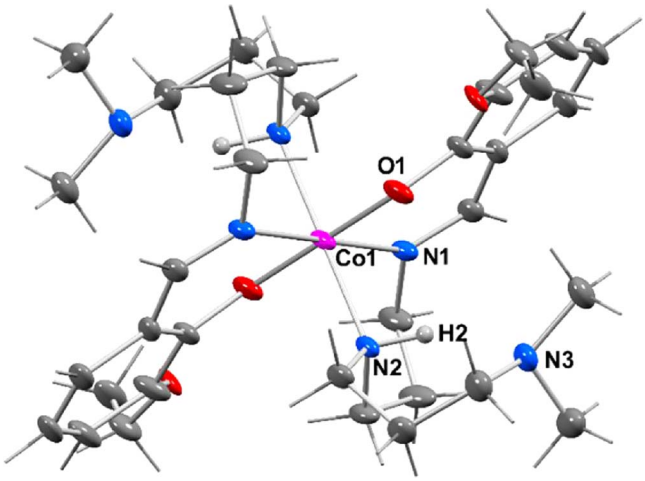

Fig. 4. Crystal structure of the complex cation of **5** with selected atom numbering scheme. Ellipsoids are drawn in 30% probability.

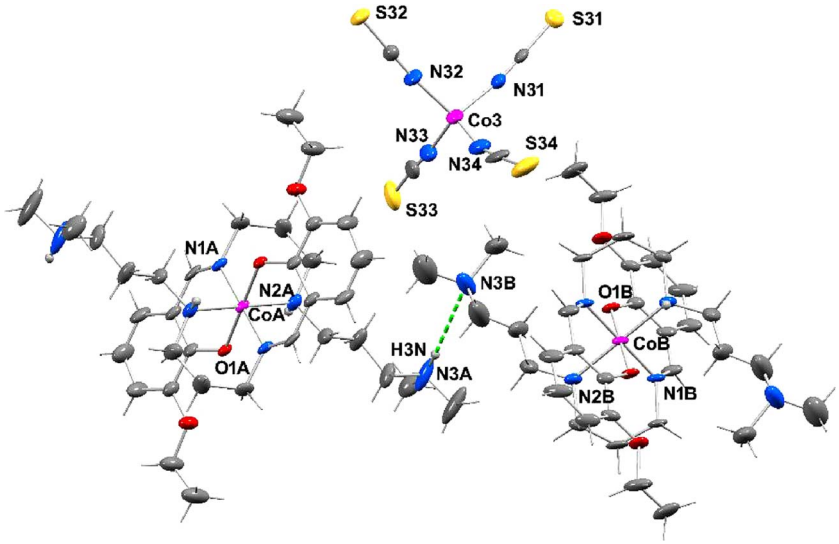

Fig. 3. Crystal structure of complex **4** displaying both crystallographically independent complex cations with selected atom labelling scheme. Ellipsoids are drawn in 30% probability.

Table 2
Selected bond distances (Å) for complexes **1–5**.[a]

Bond	1		2	3	4		5
	A	B			A	B	
Co(III)–N(imine)	1.934(4)	1.942(3)	1.924(3)	1.932(3)	1.938(5)	1.927(6)	1.940(4)
Co(III)–N(secondary amine)	2.045(4)	2.005(4)	2.012(3)	1.996(4)	2.004(6)	2.047(6)	2.012(5)
Co(III)–N(tertiary amine)	–	–	2.104(3)	2.085(4)	–		–
Co(III)–O(phenolate)	1.886(3)	1.904(3)	1.895(2)	1.844(3)	1.886(5)	1.863(4)	1.888 (4)
Co(III)–N(pseudohalide)			1.964(3)	1.916(4)	–		–
			1.948(3)	1.912(5)			
Co(II)–;1;;1;N(pseudohalide)			–	–	1.941(10)		1.956(5)
					1.955(10)		
					1.956(7)		
					1.960(8)		

[a] A and B denote two crystallographically independent components.

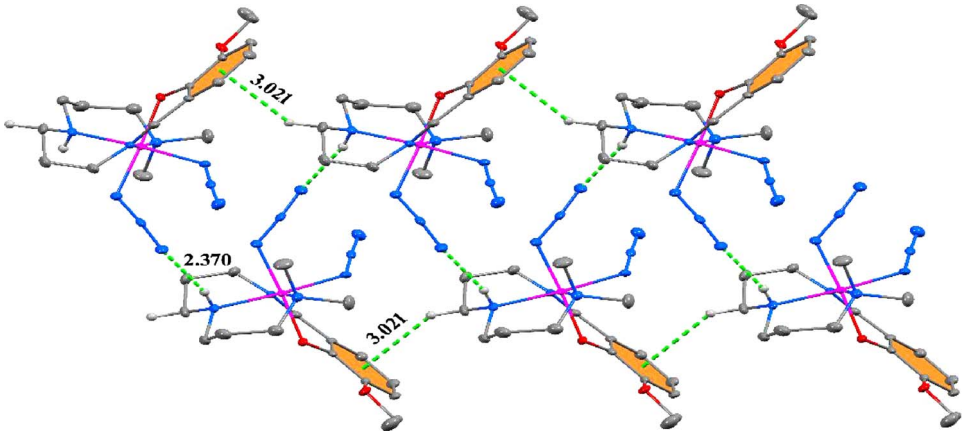

Fig. 5. A part of packing showing hydrogen bonding and C–H···π interactions in **2**.

respectively, which are usual values for low-spin octahedral Co(III) complexes [44,48,49]. In both complexes, the Co–N distances of imine, secondary and tertiary amines vary in the range 1.924(3)–1.932(3), 1.996(4)–2.012(3) and 2.085(4)–2.104(3) Å, respectively. Notably, the secondary amine bonds are somewhat longer than the imine moieties in both complexes (see Table 2), which is in accord with their respective states of hybridization. But significantly longer bond distance of tertiary amine over secondary amine group observed in these structures probably arises from the increased steric crowding at the metal centre due to the presence of two methyl substitutions at tertiary nitrogen, thereby leading to the weaker binding ability of the tertiary amine in these complexes [46]. Furthermore, the N–N distances of azide ions [1.199(4)–1.202(5) Å] that between the central nitrogen and the nitrogen connected to the metal centre are slightly longer than the terminal N–N bonds [1.157(4)–1.163(5) Å], which is the signature of the terminal azide ion [48,49]. Again, as found in similar complexes, the thiocyanate is coordinated through the nitrogen end in **3** [46,47]. The solid state structure of **2** is stabilised by hydrogen bonding interaction involving secondary amine and one of the terminal nitrogen atom of coordinated azide ion from a neighbouring molecule (see Fig. 5). The C–H···π interactions between the adjacent molecules provide further stability in the solid state in **2**. Similar type of hydrogen bonding interaction is also present in the crystal packing of complex **3** where the secondary amine hydrogen is bonded to the sulphur atom of coordinated thiocyanate ion from a neighbouring molecule. The solid state stability of the complex is further reinforced by the multiple C–H···π interaction involving two adjacent molecules (see Fig. 6).

Both **4** and **5** are ionic compounds. Complex **4** crystalizes in the monoclinic $P2_1/c$ space group in which the asymmetric unit includes two crystallographically independent complex cations of formula **[**Co(HL)(L)$]^{2+}$ on inversion centres, a $Co(NCS)_4^{2-}$ ion on a general position and a lattice water molecule with half occupancy on a general position. On the other hand, complex **5** crystalizes in the tetragonal space group $P4_2/n$ where the complex cation, **[**$Co(L)_2]^+$, resides on an inversion centre, while the complex anion, $Co(NCO)_4^{2-}$, sits on a 4-fold axis. The geometry of both $Co(NCS)_4^{2-}$ and $Co(NCO)_4^{2-}$ is tetrahedral where all the pseudohalide ions are coordinated to cobalt(II) ions through the nitrogen atoms [50–52] with the N–Co–N bond angles ranging from 105.9(3)–114.6(4) and 107.47(15)–113.6(3)° for **4** and **5**, respectively. The structures of **4** and **5** are although apparently similar, the distinction of these systems originates from the charge neutralization point of view. Crystallization of the $Co(NCS)_4^{2-}$ anion on a general position requires the protonation of tertiary amine-N of one of the Schiff base ligands for balancing the charge of the system in **4**, *i.e.*, the metal centre is coordinated to one zwitterionic and one monoanionic Schiff base ligands in the complex cation of **4**. But in complex **5**, the tertiary amine-N atoms of both Schiff base ligands are in the monoanionic form. Interestingly, in both cases, whether the Schiff base ligands are in the zwitterionic form or in the monoanionic state, coordinated to the metal centres in the tridentate fashion. In these complex cations, the geometry of cobalt(III) centre is best described as a pseudo-octahedral and it is coordinated by two Schiff base ligands, each of them occupies a facial position and binds the metal centre through phenolate-O, imine-N and secondary amine-N. The Co–N distances of imine and secondary amine and the Co–O distances of phenolate group of the Schiff base ligand in **4** and **5** span in the range 1.926(6)–1.940(4), 2.005(6)–2.050(7) and 1.862(4)–1.888(4) Å, respectively, which are comparable to bond distances observed in **1** − **3** and also to the reported low-spin octahedral Co(III) complexes with similar coordination environments [44,48,49]. Like **1** − **3**, the imine bonds are found somewhat shorter than the secondary amine nitrogen in **4** and **5** as expected. Various types of non-covalent interactions are present in the solid state in both compounds.

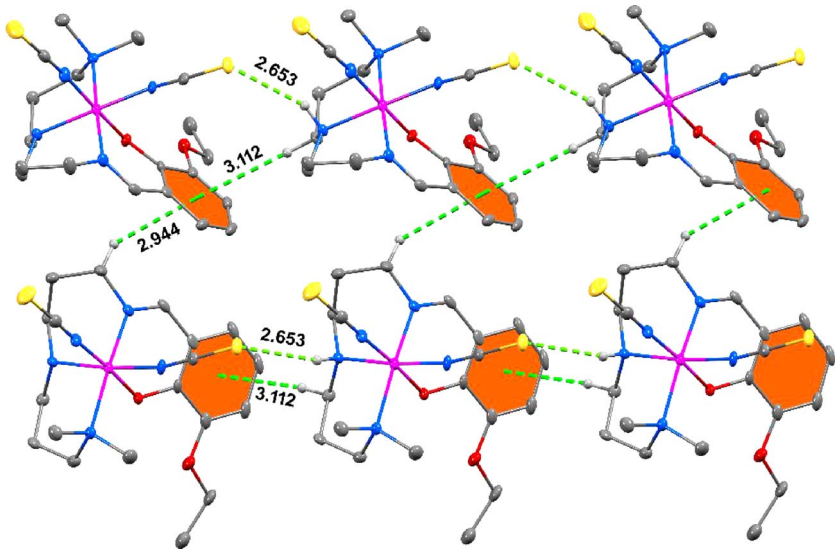

Fig. 6. A part of crystal packing of **3** showing hydrogen bonding and C–H···π interactions.

The most striking difference in the noncovalent interactions in these compounds mainly arises from the hydrogen bonding interactions. As the tertiary amine nitrogen in the Schiff base ligand is not protonated in **5**, thereby it involves in the intramolecular hydrogen bonding with secondary amine group from the same ligand (Fig. S2). On the other hand, both protonated and free tertiary amine nitrogen of the Schiff base ligands together with lattice methanol molecules engage in hydrogen bonding in **4** (Fig. S3).

Overall, several important information regarding the versatile coordination ability of the Schiff base ligand can be achieved from the X-ray structural studies in these systems. It is observed that the Schiff base ligand can either bind the metal centre in the tetradentate fashion using all the available donor sites of the monoanionic deprotonated form (in **2** and **3**) or in the tridentate fashion using the zwitterionic form of the Schiff base ligand with pendent quaternary amine nitrogen (in **1** and **4**). Moreover, the monoanionic deprotonated ligand can also bind the metal centre in the tridentate fashion (in **4** and **5**) in which the pendent tertiary amine nitrogen participates in the intramolecular hydrogen bonding. Furthermore, the facial binding of the triamine part of the Schiff base ligand to the metal centre is observed in our recently reported Ni(II) systems [46], while in **2** and **3** it is meridionally coordinated to the metal centre. Therefore, all these above adaptabilities associated with this triamine suggest that the ligand derived from this triamine could be a promising ligand for the development of the coordination chemistry with diverse structures. One more interesting aspect of the structural studies is that the influence of the counter ions is noticed in the structural diversity. What we have observed that the stronger donor ability of the counter anion (for example azide ion) helps to stabilize the system through the coordination to the metal centre, while the weaker coordinating counter ion like perchlorate, the zwitterionic anion of the Schiff base coordinates the metal centre for the stabilisation of the system. A mixed impression is observed when thiocyanate counter anion was used, and in that case influence of the solvent used for the synthesis is also observed for the ultimate stability of the system. As the cyanate ion preferably coordinates the metal centre using relatively less electronegative nitrogen donor atom that is why it could not provide sufficient electron density to the metal centre in the stability of the system.

3.3. Electrochemical studies

The reduction potential of the active site of a metalloenzyme is the crucial factor behind the catalytic oxidation of biologically important organic compounds in the living systems. Therefore, the electrochemical study of the synthetic analogues especially under the identical condition of the catalytic study is important as that could provide significant information from which one can assess the potential of the compounds as catalysts. In this regard, the cyclic voltammetric data of all complexes were recorded in methanol with 0.1 M tetrabutylammonium perchlorate as a supporting electrolyte at room temperature. The representative cyclic voltammograms of **2** and **3** are displayed in Fig. 7, while Fig. 8 represents the electrochemical behaviour of **4** and **5**. Cyclic voltammograms of **1** − **3** consist of an irreversible reduction response in the range −0.81 to −1.10 V, which is associated with the reduction of Co(III) to Co(II) at the electrode surface. Unlike **1** − **3**, the cyclic voltammograms of **4** and **5** consist of both an irreversible oxidative response (0.96 V for **4** and 0.93 V for **5**) and a reductive response (−0.97 V for **4** and −1.09 V for **5**). The reduction process is responsible for the reduction of Co(III) to Co(II) of the complex cations at the electrode surface, whereas the oxidative response is due to the oxidation of Co(II) to Co(III) of the complex anions of general formula $[CoX_4]^{2-}$ (X = SCN for **4** and NCO for **5**). Electrochemical irreversible responses for both oxidation and reduction

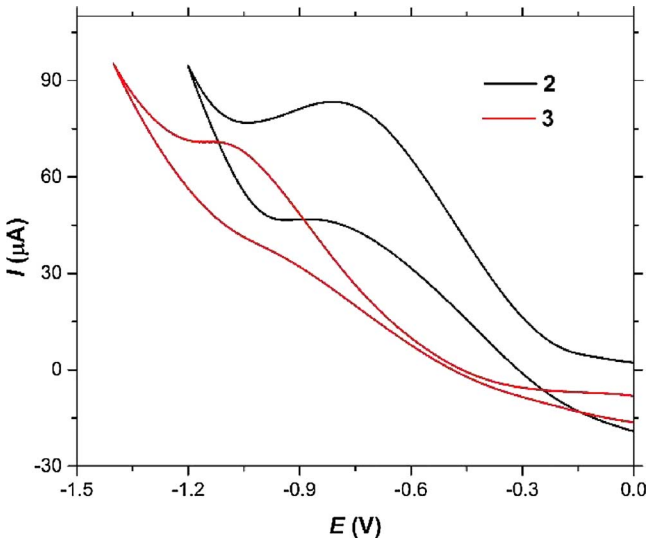

Fig. 7. Cyclic voltammograms of **2** and **3** in methanol using a platinum working electrode in the presence of tetrabutylammonium perchlorate as a supporting electrolyte at room temperature with scan rate 100 mV s^{-1}.

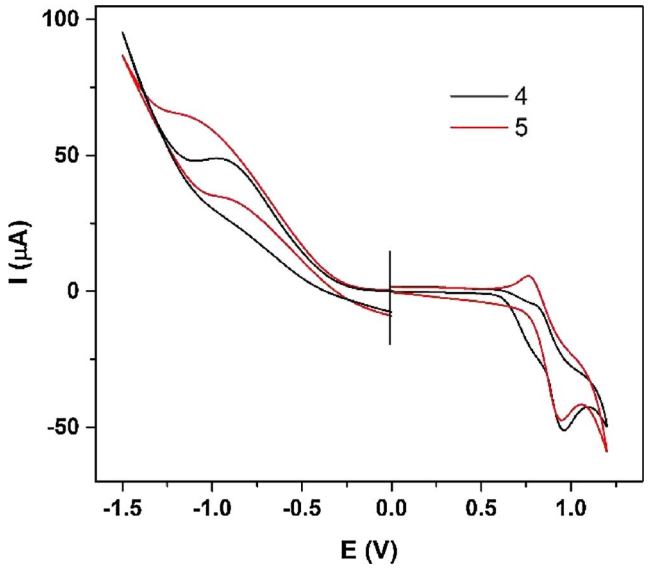

Fig. 8. Cyclic voltammograms of **4** and **5** in methanol using a platinum working electrode in the presence of tetrabutylammonium perchlorate as a supporting electrolyte at room temperature with scan rate 100 mV s^{-1}.

processes are indicative of the significant modification of the co-ordination spheres of the resulting species at the electrode surface.

3.4. Catalytic oxidation of o-aminophenol

Oxidation of *o*-aminophenol (OAPH) by molecular dioxygen in presence of catalytic amount of the complexes was studied UV–vis spectrophotometrically in dioxygen-saturated methanol at room temperature [33]. In this context, 1.0×10^{-4} M methanolic solution of the complexes were allowed to react with a 0.01 M solution of OAPH under aerobic condition. The advancement of the reaction was examined by UV–vis spectrophotometrically at 5 min time interval, and the time-dependent spectral profiles are depicted in Figs. 9–11 for **2**, **3** and **5**, respectively, and in Figs. S4 and S5 for **1** and **4**, respectively. These spectral scans reveal the cumulative development of peak intensity at *ca*. 434 nm, characteristic of phenoxazinone chromophore, that unambiguously establish that all complexes except complex **1** are efficient catalysts for the oxidation of OAPH by molecular dioxygen. Detailed

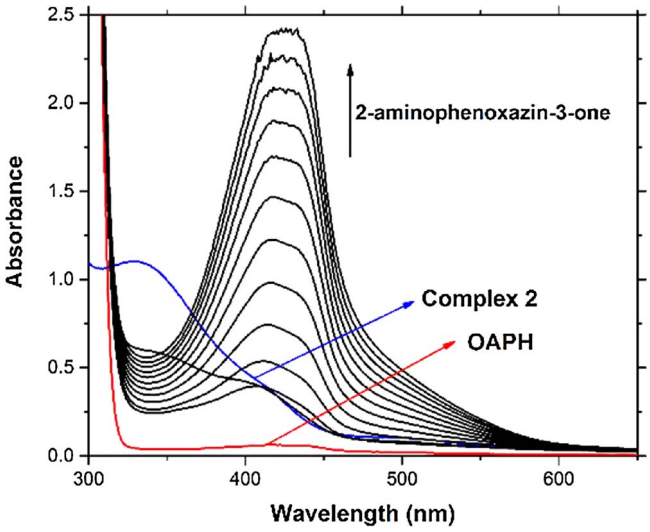

Fig. 9. Time dependent UV–vis spectral changes for the oxidation of *o*-aminophenol (1.0×10^{-2} M) catalysed by **2** (1×10^{-4} M) in dioxygen-saturated methanol. The spectra were recorded at 5 min intervals under aerobic conditions at room temperature.

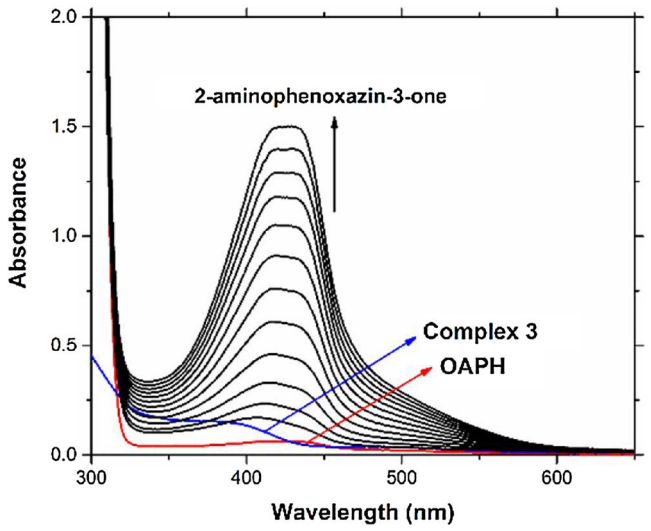

Fig. 10. Time dependent spectral scan showing growth of 2-aminophenoxazin-3-one at 434 nm upon addition of 1.0×10^{-2} M OAPH to a solution containing **3** (1×10^{-4} M) in dioxygen-saturated methanol. The spectra were recorded at 5 min intervals under aerobic conditions at room temperature.

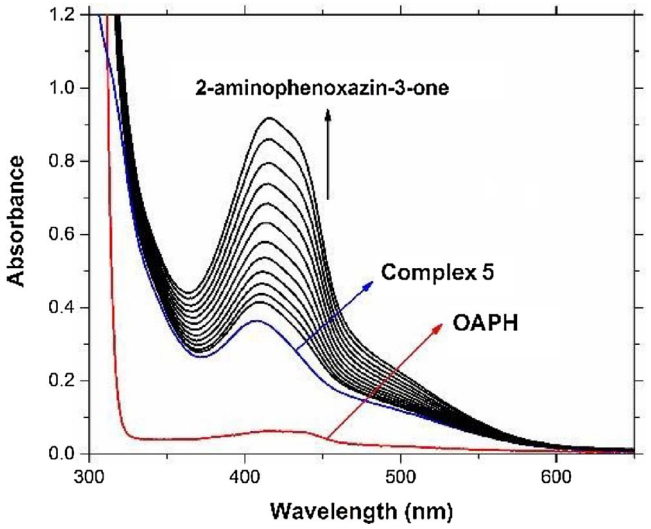

Fig. 11. The time resolved spectral profile showing oxidation of *o*-aminophenol (1.0×10^{-2} M) catalysed by **5** (1×10^{-4} M) in dioxygen-saturated methanol. The spectra were recorded at 5 min intervals under aerobic conditions at room temperature.

kinetic study is further required to get insight into the catalytic efficiency in these complexes. Accordingly, 2.0×10^{-5} M solutions of the complexes were reacted with excess substrate at the pseudo-first-order condition, and the reaction kinetics at the maximum band (434 nm) of 2-aminophenoxazin-3-one was carried out for a period of 10 min, and the initial rate was determined by linear regression from the slope of the absorbance *versus* time plot [43]. As can be seen from Fig. 12, the initial rates follow the rate saturation kinetics with increasing concentration of the substrate. These observations suggest that a complex-substrate aggregate is formed in a preequilibrium stage prior to the irreversible redox transformation of the intermediate in the rate determining step of the catalytic cycle. Michaelis-Menten model is appropriate to analyse such kinetic data to evaluate the parameters V_{max}, K_M, and K_{cat}. The observed and simulated nonlinear initial rates *versus* substrate concentration plot are shown in Fig. 12 and simulated kinetic parameters are given in Table 3. Analysis of the experimental data yielded Michaelis binding constant (K_M) value of 1.02×10^{-2}, 1.35×10^{-2}, 1.24×10^{-2}, 8.87×10^{-3} and 2.74×10^{-2} M for **1–5**, respectively, while V_{max} values of 4.64×10^{-8}, 3.11×10^{-7},

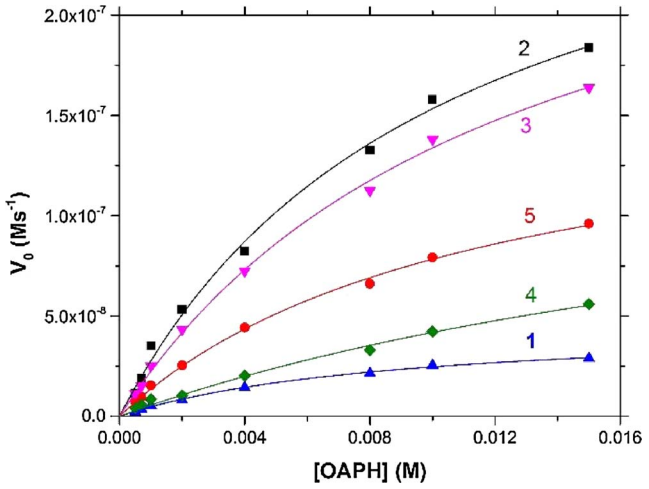

Fig. 12. Initial rate *versus* substrate concentration plot for the oxidation of OAPH in dioxygen-saturated methanol catalysed by **1–5** at room temperature. Symbols and solid lines represent the experimental and simulated profiles, respectively.

Table 3
Kinetic parameters of phenoxazinone synthase like activity for complexes **1–5**.

Catalyst	V_{max} (Ms^{-1})	K_M (M)	k_{cat} (h^{-1})
1	4.64×10^{-8}	1.02×10^{-2}	4.35
2	3.11×10^{-7}	1.35×10^{-2}	56.0
3	2.99×10^{-7}	1.24×10^{-2}	53.8
4	1.15×10^{-7}	8.87×10^{-3}	20.7
5	1.67×10^{-7}	2.74×10^{-2}	30.0

2.99×10^{-7}, 1.15×10^{-7} and 1.67×10^{-7} Ms^{-1} for **1–5**, respectively. The turnover number (k_{cat}) value is obtained by dividing V_{max} by the concentration of the complex used (2.0×10^{-5} M), and is found to be 4.35, 56.0, 53.8, 20.7 and 30.0 h^{-1} for **1–5**, respectively.

3.5. Mass spectral study

The mass spectral study could provide useful information of the intermediate species formed in a chemical reaction from which the most possible mechanism of the reaction pathway can be drawn. Therefore, the electrospray ionization mass spectral (ESI–MS positive) studies were carried out of a representative compound **3** alone and in presence of 50 equivalents of *o*-aminophenol in methanol. The ESI mass spectrum of compound **3** is displayed in Fig. S6. The basal peak of the complex alone is found at m/z = 364.28, which is assignable to the $[Co^{III}(L)-H]^+$, consistent with isotopic distribution patterns and also to the peak-to-peak separation of unity. The mass spectrum of the complex-substrate mixture (1:50 mol ratio) in methanol is displayed in Fig. 13. Interestingly, the base peak of the mass spectrum of complex alone become a minor species when it was carried out in presence of excess substrate. Remarkably, the base peak at m/z = 473.21 is a 1:1 complex-substrate intermediate of a monocationic species of formula $[Co^{III}(L)(OAP)]^+$ (calculated m/z = 473.20), ensuring the formation of a stable complex-substrate adduct. These observations establish the ease of formation of the complex-substrate aggregate, exploiting the stronger chelating ability of *o*-aminophenolate ion by the replacement of terminal thiocyanate ions. The peak at m/z = 213.35 is related to a protonated species of the product 2-aminophenoxazin-3-one (calculated m/z = 213.07). The peak at m/z = 216.39 is deserved to be special mention as that is related to the molecular ion peak of an important reactive intermediate **I-B** (calculated m/z = 216.09) produced during the course of oxidative coupling of *o*-aminophenol as drown in Scheme 2. This kind of information was not readily available from the literature reports on the synthetic models of phenoxazinone synthase, and in some cases even it was wrongly assigned [53]. Therefore, the present observation with careful assignment could provide useful information regarding the mechanistic pathway of functioning phenoxazinone synthase activity.

3.6. Influence of first and second coordination spheres

Although the reduction potential of the cobalt(III) centre in these complexes are very close enough, the spectral scan as well as detailed kinetic analysis reveal that **2** and **3** are efficient catalysts for the aerobic oxidation of *o*-aminophenol, and **4** and **5** are moderately reactive, while compound **1** is feebly reactive. Higher reactivity of **2** and **3** is mainly because of the availability of labile sites (azide ions in **2** and thiocyanate ions in **3**) at the first coordination sphere for the substrate binding. Somewhat greater reactivity of azide complex (**2**) compared to thiocyanate analogue (**3**) is perhaps due to the better lability of azide over thiocyanate ion. At this juncture, both the mass spectral and kinetic studies convincingly conclude that the catalytic cycle for the aerobic oxidation of *o*-aminophenol catalysed by **2** and **3** begins with the formation of a stable complex-substrate aggregate by the substitution of coordinated pseudohalides by *o*-aminophenol. This complex-substrate intermediate in the subsequent rate determining step produces OAP radical through the inner sphere electron transfer from *o*-amionophenolate to the cobalt(III) centre with the concomitant production of hydrogen peroxide in expense of regeneration of catalyst by molecular oxygen. The formation of hydrogen peroxide during the catalytic reaction was verified by the iodometric method as reported earlier [54]. The generated OAP radical thereafter produces *o*-benzoquinone monoamine (BQMI) in several ways including the disproportionation of the OAP radical itself. This BQMI is then combined with another OAPH to produce a reactive intermedia **I-B** as supported by the mass spectral study, followed by two electrons oxidation with molecular oxygen to produce another reactive intermediate **II-B**, which finally produces 2-aminophenoxazin-3-one through the oxidative dehydrogenation of intermediate **II-B** as shown in Scheme 2.

The lower reactivity of the other compounds compared to **2** and **3** is perhaps because of unavailability of the substrate binding sites at the metal centre, leading to the electron transfer through the outer sphere electron transfer mechanism. Literature reports reveal that these types of complexes are often found inactive or feebly active as observed in compound **1** [55], but in the present case, both **4** and **5** are significantly catalytically active towards the oxidation of *o*-aminophenol. We have recently observed the influence of the positive charge at the ligand backbone which brings significantly enhanced catalytic activity in the system, where the positive charge of pyridinium moiety at ligand backbone may attract the substrate OAPH towards the formation of the complex-substrate aggregate and also provides additional stability of the intermediate species through noncovalent interactions, leading to the enhanced catalytic activity [56]. In the present case, the pendent tertiary amine group is fully protonated in **1** and partially protonated in **4**, while it is not protonated in **5**. If simply the positive charge at the second coordination sphere be the crucial factor, then **1** and **4** would exhibit the enhanced catalytic activity over complex **5**. But the reactivity order of **5** > **4** > > **1** clearly suggests that some other factor is responsible for the relative catalytic ability of these complexes. In order to analyse the influence of the protonation/deprotonation at the second coordination sphere on the catalytic activity, a different set of 2×10^{-5} M solutions of **1** in methanol were prepared with varying amount of tetrabutylammonium hydroxide base, and then these resulting complex solutions were combined with 0.01 M solution of the substrate, and the reaction kinetics was monitored UV–vis spectrophotometrically. Remarkably, the catalytic activity of **1** increases with increase in the added base (Fig. 14) and finally the rate of the reaction of **1** become comparable to the rate of **5**. This observation suggests that the deprotonation of quaternary amine at the second coordination sphere favours the catalytic activity in these systems. Therefore, the

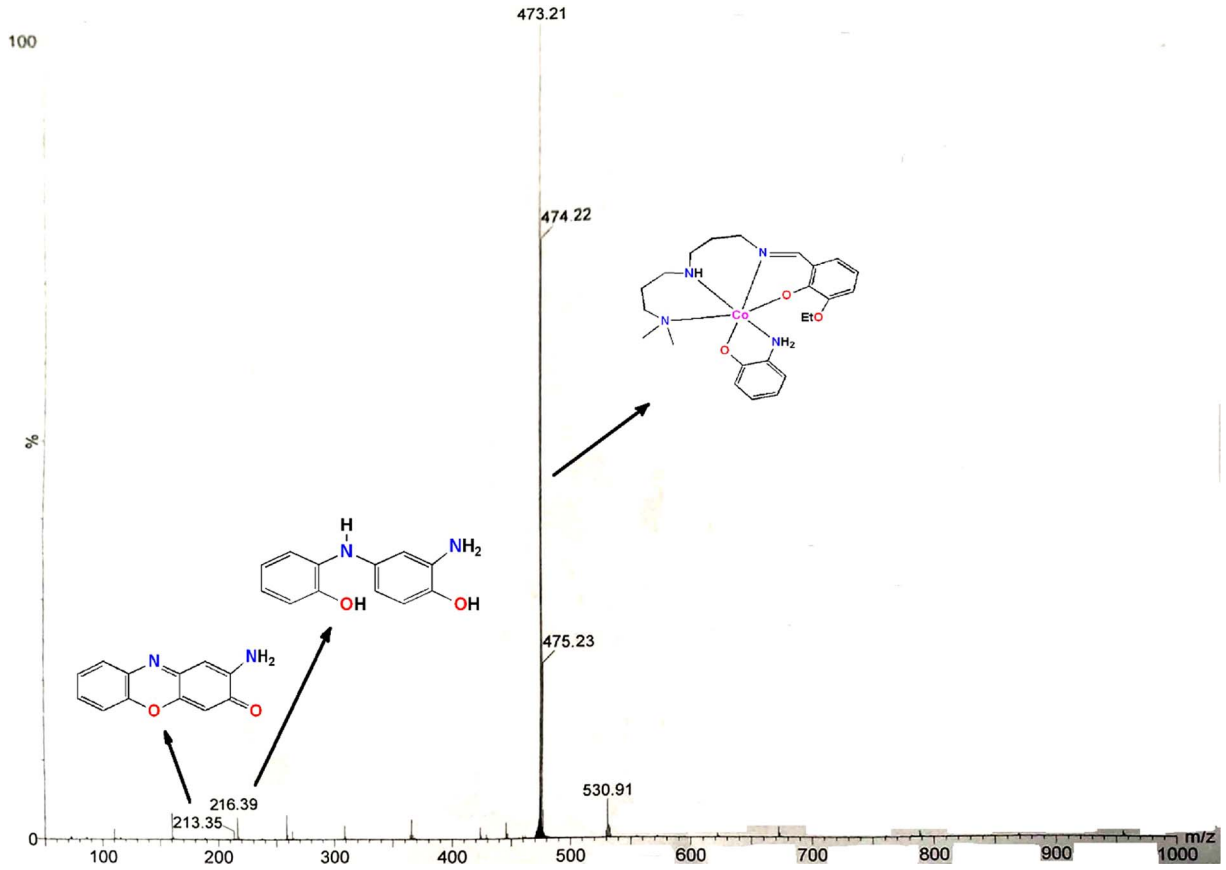

Fig. 13. Electrospray ionization mass spectrum (ESI–MS positive) of a 1:50 mixture of complex **3** and *o*-aminophenol in methanol recorded after 10 min of mixing.

present result discloses that not the positive charge but the hydrogen bond acceptor ability at the second coordination sphere is the essential criteria for the substrate recognition and stability of the intermediate for enhanced catalytic activity (see Scheme 3). Moreover, tertiary amine nitrogen abstracts proton from *o*-aminophenol and thereby facilitates the oxidation of OAPH, leading to the formation of OAP radical at the rate determining step. When tertiary amine is protonated, such proton abstraction from the substrate is not permitted and thus oxidation of *o*-aminophenol is not favoured. Therefore, the present study establishes that if the strong hydrogen bond acceptor centre is present at secondary coordination sphere that can not only recognize the substrate and stabilize the complex substrate intermediate through hydrogen bonding, but also abstract proton from the substrate, leading to the facile oxidation of the substrates like *o*-aminophenol. This result clearly justifies the fact that the extraordinary reactivity of metalloenzymes in the biological kingdom is not only associated with the availability of the labile position(s) for the substrate binding but also due to the involvement of protein chain for the substrate recognition and stabilisation of the intermediate by execution of various non-covalent interactions.

3.7. Studies with other substrates

In order to check a wider scope of substrate oxidation abilities, the reactions of 3,5-di-*tert*-butylcatechol and 2-amino-5-methylphenol with dioxygen in presence of the most reactive catalyst **2** were also investigated under the identical conditions as stated earlier (Scheme 4). From the time dependent spectral profile (Fig. 15), it is found that compound **2** is catalytically inactive towards the oxidation of 3,5-di-*tert*-butylcatechol as a cumulative increase of spectral intensity at 400 nm, characteristic for 3,5-di-*tert*-butylquinone, was not observed. However, the appearance of the isosbestic points in the spectral profile clearly suggests the binding ability of catechol towards the metal centre. Higher reduction potential *i.e.*, a lower electron donating character of 3,5-di-*tert*-butylcatechol compared to *o*-aminophenol substrate is the main reason behind the catecholase inactivity of compound **2**. On the other hand, compound **2** is found to be an efficient catalyst for the aerobic oxidation of 2-amino-5-methylphenol. As shown in Fig. 15, the cumulative growth of peak intensity at *ca.* 402 nm, characteristic for dihydro-2-aminophenoxazinone chromophore, was observed when 5.0×10^{-5} M methanolic solution of **2** was allowed to react with a 0.01 M solution of 2-amino-5-methylphenol in aerobic condition [43]. This result indicates the catalytic formation of 4a,7-dimethyldihydro-2-aminophenoxazinone in aerobic condition. Interestingly, the presence of methyl substitution does not inhibit the coupling of two aminophenols, but the final 2-electrons oxidation was blocked by methyl substitution at C4a, leading to the formation of 4a,7-dimethyldihydro-2-aminophenoxazinone instead of 2-aminophenoxazinone which is the final oxidation product of *o*-aminophenol itself. From the mass spectral study, formation of the complex-substrate adduct and the final product were clearly identified (Fig. S7). Detailed kinetic study (Fig. S8) along with the spectral scan as shown in Fig. 15 clearly indicate that catalytic oxidation of 2-amino-5-methylphenol ($V_{max} = 3.92 \times 10^{-7}$ Ms^{-1}; $k_{cat} = 70.6\ h^{-1}$) is even faster than *o*-aminophenol, which is quite reasonable as the methyl substitution at aromatic ring favours the oxidation of the substituted aminophenol.

4. Conclusions

We have successfully synthesized a new tetradentate N_3O donor Schiff base ligand from the condensation of *N,N*-dimethyldipropylenetriamine and 3-ethoxysalicylaldehyde. This Schiff base ligand was thereafter utilized for the preparation of five new cobalt complexes in the presence of different counter ions. Although stoichiometric ratios

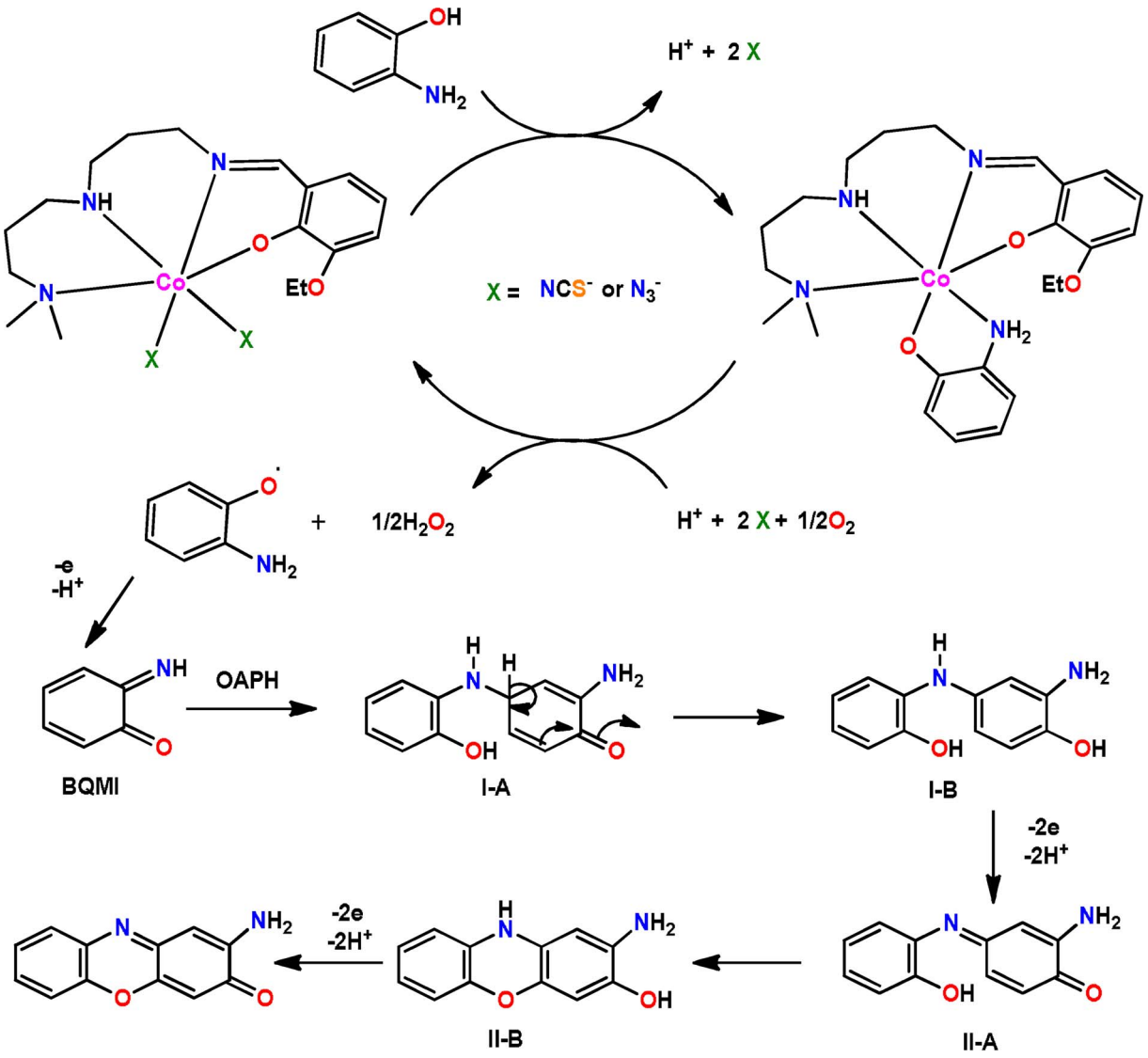

Scheme. 2. Plausible mechanistic pathway for the aerobic oxidation of *o*-aminophenol catalysed by **2** and **3**.

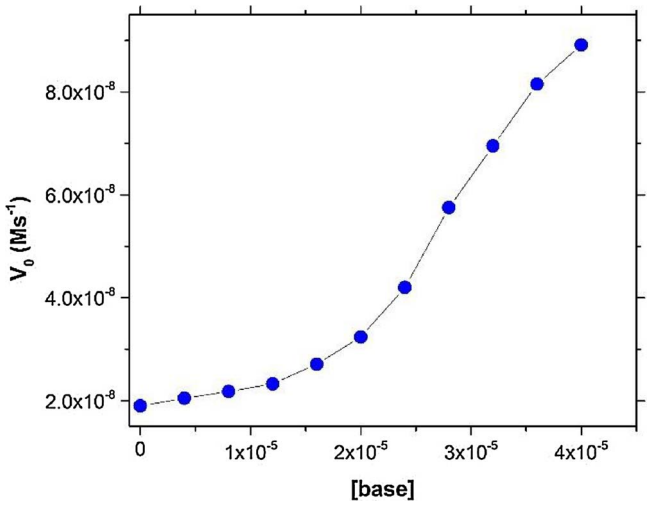

Fig. 14. Plot of initial rate *vs* concentration of an added base for the aerobic oxidation of *o*-aminophenol (0.01 M) catalysed by complex **1** (2×10^{-5} M).

did not have any effect in the formation of these compounds, the role of the solvent and counter anions was noticed for their synthesis (**3** *versus* **4**). X-ray crystal crystallography disclosed that the Schiff base can coordinate the metal centre either in the tetradentate fashion through monoanionic deported form using all the available donor sites (in **2** and **3**) or in the tridentate fashion using the zwitterionic form of the Schiff base ligand with pendent quaternary amine nitrogen (in **1** and **4**). Moreover, the tridentate binding ability of the monoanionic deprotonated ligand to the metal centre was also observed (in **4** and **5**), in which the pendent tertiary amine nitrogen participates in the intramolecular hydrogen bonding. It is to be noted that the facial binding mode of the triamine part of the Schiff base ligand was observed in our recent report with Ni(II) system, while it is meridionally coordinated to the metal centre in the present systems (**2** and **3**). All these adaptabilities of this triamine make it as a promising candidate for exploration of the coordination chemistry with diverse structures. All complexes except **1** exhibit strong phenoxazinone synthase mimicking activity, where the available binding sites at the first coordination sphere of the metal centre for substrate binding is the main reason for significantly higher catalytic activity in **2** and **3**. Although, compound **1** is found almost inactive, the presence of hydrogen bond acceptor site at the second coordination sphere in both **4** and **5** make them effective candidates for phenoxazinone synthase activity. Interestingly, this

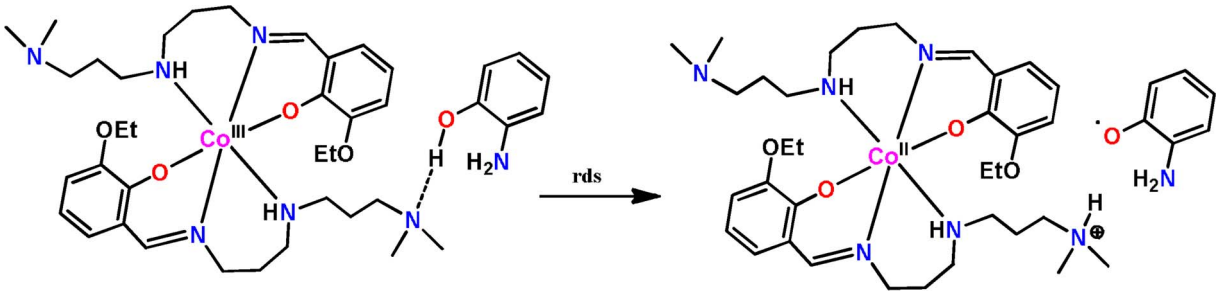

Scheme 3. Stabilization of intermediate through hydrogen bonding and facilitating oxidation of *o*-aminophenol by proton abstraction.

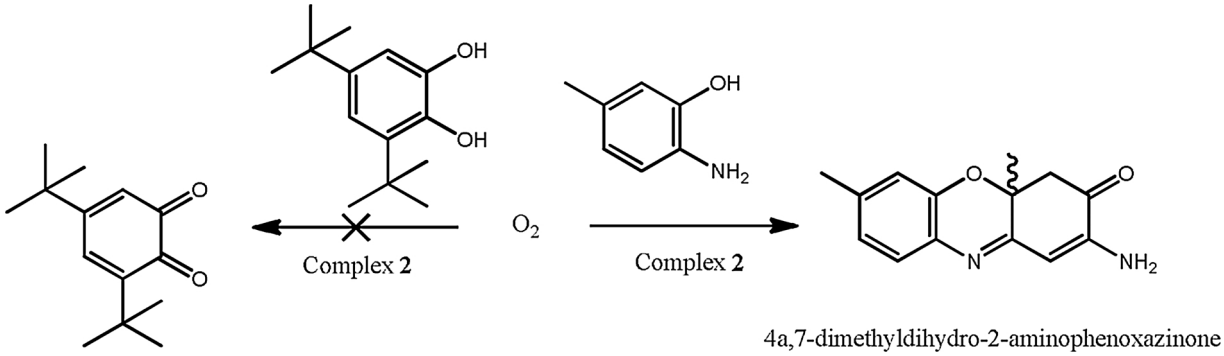

Scheme 4. Reaction of substituted catechol and substituted *o*-aminophenol with oxygen.

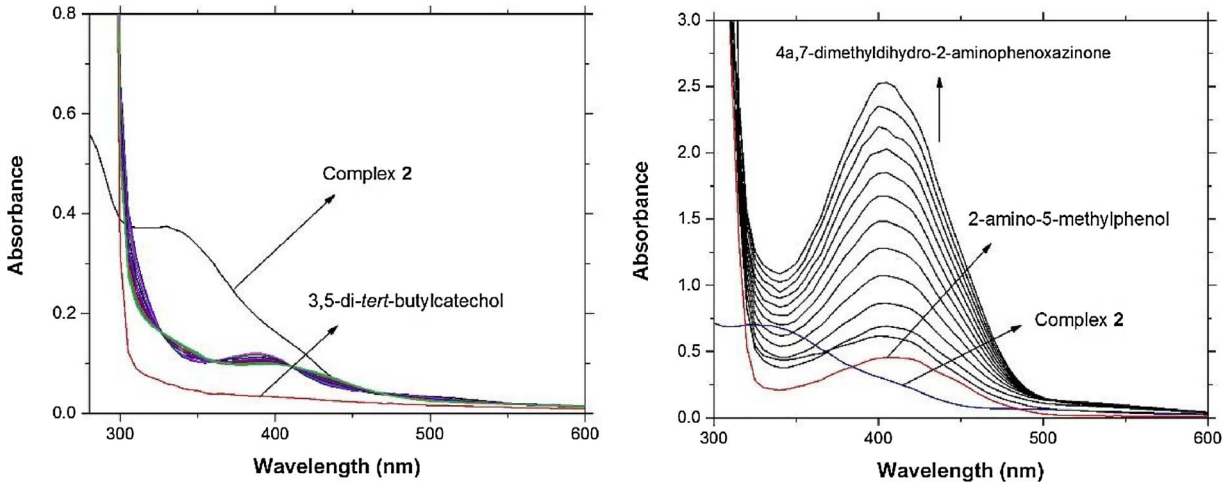

Fig. 15. Reactions of 3,5-di-*tert*-butylcatechol (1.0×10^{-2} M) and 2-amino-5-methylphenol (1.0×10^{-2} M) with dioxygen in presence of the most reactive catalyst **2** (5.0×10^{-5} M) in methanol.

hydrogen bond acceptor site not only stabilizes the complex-substrate aggregate through hydrogen bonding but also abstracts proton from *o*-aminophenol, thereby facilitating oxidation of the substrate. The mass spectral study of **3** in the presence excess substrate disclosed some important intermediates, which is helpful to get insight into the mechanistic pathway of functioning phenoxazinone synthase activity. These results overall highlight the importance of the labile or vacant positions at the first coordination sphere available for substrate binding and the substrate recognition cum proton abstraction centre at the second coordination sphere for the development of the better *in vitro* catalysts as that have a high degree of structural resemblance with the metalloenzymes. Finally, in order to increase scope of substrate oxidation abilities, the reactions of 3,5-di-*tert*-butylcatechol and 2-amino-5-methylphenol with dioxygen were investigated in presence of **2**. Although it is not an active catalyst for oxidation of substituted catechol but is proved to be an efficient catalyst for the oxidation of substituted *o*-aminophenol in aerobic condition. Interestingly, in both cases, the substrate binding ability to the metal centre was experimentally established.

Acknowledgements

A.P. would like to thank the University Grant Commission, New Delhi (Sanction no. PSW-229/15-16) for financial support. The authors thank Indian Institute of Chemical Biology, Kolkata for providing the Mass spectral facility.

Appendix A. Supplementary data

Supplementary data associated with this article can be found, in the online version, at http://dx.doi.org/10.1016/j.mcat.2018.02.013.

References

[1] S.I. Murahashi, Y. Imada, 2nd edn, M. Beller, C. Bolm (Eds.), Transition Metals for Organic Synthesis, vol. 2, Wiley-VCH, Weinheim, Germany, 2004, p. 497.
[2] J. Gómez, G. Garcia-Herbosa, J.V. Cuevas, A. Arnáiz, A. Carbayo, A. Muñoz, L. Falvello, P.E. Fanwick, Inorg. Chem. 45 (2006) 2483–2493.
[3] T. Funabiki (Ed.), Dioxygenases in Catalysis by Metal Complexes, Oxygenases and Model Systems, Kluwer Academic, Dordrecht, 1997, p. 19.
[4] J.P. Klinman, J. Biol. Inorg. Chem. 16 (2011) 1.
[5] I. Bertini, H.B. Gray, S.J. Lippard, J.S. Valentine (Eds.), Dioxygen Reactions in Bioinorganic Chemistry, University Science Books, Sausalito, 1994, p. 253.
[6] The chemistry and activation of dioxygen species (O_2, O_2^- and H_2O_2) in biology, in: A.E. Martell, D.T. Sawyer (Eds.), Oxygen Complexes and Oxygen Activation by Transition Metals, Plenum, New York, 1988, p. 131.
[7] E.I. Solomon, T.C. Brunold, M.I. Davis, J.N. Kemsley, S.K. Lee, N. Lehnert, F. Neese, A.J. Skulan, Y.S. Yang, J. Zhou, Chem. Rev. 100 (2000) 235–350.
[8] E.I. Solomon, R. Sarangi, J.S. Woertink, A.J. Augustine, J. Yoon, S. Ghosh, Acc. Chem. Res. 40 (2007) 581–591.
[9] E.G. Kovaleva, J.D. Lipscomb, Nat. Chem. Biol. 4 (2008) 186–193.
[10] S.S. Stahl, Science 309 (2005) 1824–1826.
[11] L.I. Simándi (Ed.), Advances in Catalytic Activation of Dioxygen by Metal Complexes, Springer, New York, 2003.
[12] B. Meunier (Ed.), Biomimetic Oxidations Catalyzed by Transition Metal Complexes, Imperial College, London, 2000.
[13] P. Chaudhuri, K. Wieghardt, Prog. Inorg. Chem. 50 (2001) 151–216.
[14] R.H. Holm, E.I. Solomon, Chem. Rev. 104 (2004) 347–1200.
[15] C. Mukherjee, T. Weyhermüller, E. Bothe, E. Rentschler, P. Chaudhuri, Inorg. Chem. 46 (2007) 9895–9905;
M. Mitra, T. Kundu, G. Kaur, G. Sharma, A.R. Choudhury, Y. Singh, R. Ghosh, RSC Adv. 6 (2016) 58831–58838.
[16] P. Chaudhuri, K. Wieghardt, T. Weyhermüller, T.K. Paine, S. Mukherjee, C. Mukherjee, Biol. Chem. 386 (2005) 1023–1033.
[17] U. Jhan, Top. Curr. Chem. 320 (2004) 323–452.
[18] S.E. Allen, R.R. Walvoord, R. Padilla-Salinas, M.C. Kozlowski, Chem. Rev. 113 (2013) 6234–6458.
[19] T.K. Paine, L. Que Jr., Struct. Bond. 160 (2014) 39–56.
[20] W. Zhang, W. Lai, R. Cao, Chem. Rev. 117 (2017) 3717–3797;
S. Wang, S.-Y. Chen, X.-Q. Yu, Chem. Commun. 53 (2017);
M. Yamashita, Bull. Chem. Soc. Jpn. 89 (2016) 269–281.
[21] N.C. Jana, P. Brandão, A. Panja, J. Inorg. Biochem. 159 (2016) 96–106.
[22] A. Panja, N.C. Jana, A. Bauzá, S. Adak, T.M. Mwania, D.M. Eichhorn, A. Frontera, Chem. Select. 2 (6) (2017) 2094–2105.
[23] A. Panja, P. Guionneau, Dalton Trans. 42 (2013) 5068–5075;
A. Panja, N.C. Jana, P. Brandão, New J. Chem. 41 (2017) 9784–9795.
[24] A. Panja, RSC Adv. 4 (2014) 37085–37094;
N.C. Jana, P. Brandão, A. Bauzá, A. Frontera, A. Panja, J. Inorg. Biochem. 176 (2017) 77–89.
[25] C.E. Barry, P.G. Nayar, T.P. Begley, J. Am. Chem. Soc. 110 (1988) 3333–3342.
[26] E. Frei, Cancer Chemo Ther. Rep. Part 1 58 (1974) 49–54.
[27] U. Hollstein, Chem. Rev. 74 (1974) 625–652.
[28] L.I. Simándi, T.M. Simándi, Z. May, G. Besenyei, Coord. Chem. Rev. 245 (1) (2003) 85–93.
[29] M. Hassanein, M. Abdo, S. Gerges, S. El-Khalafy, J. Mol. Catal. A: Chem. 287 (1) (2008) 53–56.
[30] T.M. Simándi, L.I. Simándi, M. Győr, A. Rockenbauer, Á. Gömöry, Dalton Trans. 7 (2004) 1056–1060.
[31] T. Horváth, J. Kaizer, G. Speier, J. Mol. Catal. A: Chem. 215 (1) (2004) 9–15.
[32] J. Kaizer, G. Baráth, R. Csonka, G. Speier, L. Korecz, A. Rockenbauer, L. Párkányi, J. Inorg. Biochem. 102 (4) (2008) 773–780.
[33] S.K. Dey, A. Mukherjee, Coord. Chem. Rev. 310 (2016) 80–115.
[34] S. Sagar, S. Sengupta, A.J. Mota, S.K. Chattopadhyay, A.E. Ferao, E. Riviere, W. Lewis, S. Naskar, Dalton Trans. 46 (2017) 1249–1259.
[35] A. Jana, N. Aliaga-Alcalde, E. Ruiz, S. Mohanta, Inorg. Chem. 52 (2013) 7732–7746.
[36] P. Mahapatra, S. Ghosh, S. Giri, V. Rane, R. Kadam, M.G.B. Drew, A. Ghosh, Inorg. Chem. 56 (9) (2017) 5105–5121.
[37] L.A. Joyce, S.H. Shabbir, E.V. Anslyn, Chem. Soc. Rev. 39 (2010) 3621–3632.
[38] J. Meeuwissen, J.N.H. Reek, Nat. Chem. 2 (2010) 615–621.
[39] J.V. Bannister, W.H. Bannister, G. Rotilio, CRC Crit. Rev. Biochem. 22 (1987) 111–180.
[40] A. Company, L. Gomez, R. Mas-Balleste, I.V. Korendovych, X. Ribas, A. Poater, T. Parella, X. Fontrodona, J. Benet- Buchholz, M. Sola, L. Que Jr., E.V. Rybak-Akimova, M. Costas, Inorg. Chem. 46 (2007) 4997–5012.
[41] G.M. Sheldrick, SADABS, University of Göttingen, Germany, 1996.
[42] G.M. Sheldrick, Acta Crystallogr. Sect. A: Found. Crystallogr. 64 (2008) 112–122.
[43] A.C. Sousa, M.C. Oliveira, L.O. Martins, M.P. Robalo, Green Chem. 16 (2014) 4127–4136;
C.E. Barry, P.G. Nayar, T.P. Begley, Biochemistry 28 (1989) 6323–6333.
[44] A. Panja, Dalton Trans. 43 (2014) 7760–7770.
[45] M. Shyamal, T.K. Mandal, A. Panja, A. Saha, RSC Adv. 4 (2014) 53520–53530.
[46] A. Panja, N.C. Jana, S. Adak, P. Brandão, L. Dlháň, J. Titiš, R. Boča, New J. Chem. 41 (2017) 3143–3153.
[47] A. Hazari, L.K. Das, A. Bauzá, A. Frontera, A. Ghosh, Dalton Trans. 45 (2016) 5730–5740.
[48] A. Panja, M. Shyamal, A. Saha, T.K. Mandal, Dalton Trans. 43 (2014) 5443–5452.
[49] L. Mandal, S. Mohanta, Dalton Trans. 43 (2014) 15737–15751.
[50] H. Mori, N. Sakurai, S. Tanaka, H. Moriyama, T. Mori, H. Kobayashi, A. Kobayashi, Chem. Mater. 12 (2000) 2984–2987.
[51] S. Sen, P. Talukder, S.K. Dey, S. Mitra, G. Rosair, D.L. Hughes, G.P.A. Yap, G. Pilet, V. Gramlich, T. Matsushita, Dalton Trans. (2006) 1758.
[52] A. Ray, G.M. Rosair, R. Kadam, S. Mitra, Polyhedron 28 (2009) 796–806.
[53] N. Sarkar, K. Harms, A. Bauzá, A. Frontera, S. Chattopadhyay, Chem. Select. 2 (2017) 2975–2984.
[54] J. Adhikary, A. Chakraborty, S. Dasgupta, S..l.K. Chattopadhyay, R. Kruszynski, A. Trzesowska-Kruszynska, S. Stepanović, M. Gruden-Pavlović, M. Swart, D. Das, Dalton Trans. 45 (2016) 12409–12422.
[55] K. Ghosh, K. Harms, S. Chattopadhyay, Polyhedron 112 (2016) 6–17.
[56] A. Panja, N.C. Jana, M. Patra, P. Brandão, C.E. Moore, D.M. Eichhorn, A. Frontera, J. Mol. Catal. A Chem. 412 (2016) 56–66.